# Supplementary materials for

## A carbon dot-based metal-free photocatalyst enables $O_2$ to serve as both reactant and electron sink for enhancing $H_2O_2$ photoproduction

*Jiaxuan Wang [a], Yan Liu [a], Yidong Han [a], Kaili Bao [a], Tiwei He [a], Hui Huang [a], Yang Liu *[a] and Zhenhui Kang *[a, b]*

[a] Institute of Functional Nano & Soft Materials (FUNSOM), Jiangsu Key Laboratory for Carbon-Based Functional Materials & Devices, Soochow University, 199 Ren'ai Road, Suzhou, 215123, Jiangsu, China.

[b] Macao Institute of Materials Science and Engineering (MIMSE), MUST-SUDA Joint Research Center for Advanced Functional Materials, Macau University of Science and Technology, Taipa 999078, Macao, China.

*Correspondence: yangl@suda.edu.cn; zhkang@suda.edu.cn

## Experimental Section

### S1. Materials

All these materials were used directly without any treatment. Nitrogen and oxygen (98%) were purchased from Adamas. Anhydrous acetonitrile was purchased from J&K. $KMnO_4$ titration standard solution (0.004 mol/L) was purchased from AKX.

### S2. Characterization

The crystal structure of the as-prepared products was characterized by power X-ray diffraction (XRD) through a PIXcel3D X-ray diffractometer (Empyrean, Holland Panalytical) equipped with Cu Kα radiation ($\lambda$ = 0.154 nm). The morphology of the samples was characterized by scanning electron microscopy (SEM). Transmission electron microscopy (TEM) and high-resolution transmission electron microscopy (HRTEM) were observed by FEI-Tecnai TF20 transmission electron microscope (200 kV accelerating voltage). The UV–vis absorption spectrum was measured by a UV-VIS-NIR Spectrophotometer (Lambda 950, PerkinElmer). Raman spectrum was carried out on a Raman spectrometer (Horiba HR800). Fourier transform infrared (FT-IR) spectroscopy was performed on a Hyperion spectrometer (Bruker, Germany) with a scan range of 400-4000 $cm^{-1}$. X-ray photoelectron spectroscopy (XPS) measurement was conducted on an Escalab 250Xi X-ray photoelectron spectroscope (Thermo Fisher Scientific, America) with a monochromatic Al Kα X-ray source. All electrochemical measurements were conducted on a CHI 760E workstation (CH Instruments, Shanghai, China). Electrochemical impedance spectra (EIS) measurements were carried out at open circuit potential with a frequency range from 1 MHz to 0.01 Hz in ultrapure water. The photo-response performance was obtained at open circuit potential in 0.1 M sodium sulfate ($Na_2SO_4$).

### S3. Measurement of photocatalytic properties

Experiments for the production of $H_2O_2$ by photocatalysis were carried out in a quartz bottle containing 10 mg of catalyst, ultrapure water (40 mL) without any sacrificial agent. The suspension was continuously stirred under light ($\lambda \geq 420$ nm) for 1 h in air by a multi-channel photochemical reaction system (PCX 50B, Beijing perfect-light Co., Ltd, China). Then, the reaction solution was centrifuged, and the obtained solution was

filtered through a filter. Finally, the photocatalytic activity was evaluated by measuring the amount of $H_2O_2$ generated in the supernatant by titration with potassium permanganate. The photocatalytic performance test under saturated $O_2$ and saturated $N_2$ is to continuously blow high-purity $O_2$ and high-purity $N_2$ into the test solution for 0.5 h, and then carry out the photocatalytic test.

**S4. Transient photovoltage measurements**

The transient photovoltage (TPV) responses were conducted on a home-made measurement system. The excitation source was a laser radiation pulse from a third harmonic Nd: YAG laser (Beamtech Optronics Co., Ltd) (wavelength of 355 nm and the repetition rate is 5 Hz). The TPV signal was registered by a 5 GHz digital oscilloscope (MDO3104, Tektronix). The signal of the TPV was first amplified and then recorded by an oscilloscope. All measurements were performed at room temperature and ambient pressure. The electrode covered with the sample was used as the working electrode, and the platinum wire was used as the counter electrode. The *in situ* TPV experiment used the FTO glass of the deposited sample as the working electrode, and tested under different conditions (anhydrous acetonitrile solution saturated with oxygen or nitrogen, acetonitrile solution with 0.5 vol% water/acetonitrile acetonitrile).

**S5. Transient photocurrent responses (TPR) measurement**

The TPR measurement was conducted with a three electrodes system. The test was performed at the open circuit potential with a 30-second light on/off cycle ($\lambda \geq 420$ nm). Typically, L-type glassy carbon electrodes were used as the working electrodes, which were loaded with DEX-0 and DEX-160 (100 μg $cm^{-2}$). The carbon rod was treated as the counter electrode and the saturated calomel electrode (SCE) was used as the reference electrode. The light is provided by a Xe lamp with a 420 nm filter.

**S6. Electrochemical impedance spectroscopy (EIS) measurement**

The EIS was measured in a water solution with a three electrodes system at the open circuit potential. The glassy carbon electrode (GCE) coated with different catalysts (100 μg·$cm^{-2}$) was used as the working electrode. The carbon rod and saturated calomel electrode (SCE) were served as the counter electrode and the reference electrode. High

frequency: 106 Hz, low frequency: 0.01 Hz.

**S7. Determination of apparent quantum efficiency (AQE)**

The following is the calculation of the AQE at λ = 365 nm for DEX-160.

20 mg catalyst, one magneton and 45 mL ultrapure water were added to the light reactor and stirred at room temperature for 1.5 h. The average intensity of irradiation was determined to be 65 mW/cm$^2$ and the irradiation area was 18 cm$^2$. The number of incident photons (N) is calculated by equation (1). The quantum efficiency is calculated by equation (2).

$$N = \frac{E\lambda}{hc} \tag{1}$$

$$QE = \frac{2 \times the\ number\ of\ evolved\ H_2O_2}{the\ number\ of\ incident\ photons} \times 100\% \tag{2}$$

$h$ is plank constant ($6.626\times10^{-34}$ J·s = $4.136\times10^{-15}$ eV·s), c is the speed of light ($3.0\times10^{8}$ m·s$^{-1}$), and $\lambda$ is the wavelength of light (420, 500, 590 and 660 nm) and $N_A$ is Avogadro number ($6.02\times10^{23}$).

**S8. Determination of electron transfer number and selectivity.**

The calculation formula is as follow:

$$n = \frac{4\Delta I_d}{\Delta I_d + \frac{\Delta I_r}{N}} \tag{3}$$

$$H_2O_2\ (\%) = \frac{200\frac{\Delta I_r}{N}}{\Delta I_d + \frac{\Delta I_r}{N}} \tag{4}$$

$\Delta I_d$ and $\Delta I_r$ correspond to the current difference on the disk and ring electrodes in light, respectively, and N equals to 0.43 representing the collection coefficient of the RRDE electrode. The rotating ring disk electrode covered with the sample on the disk was used as the working electrode, and the saturated calomel electrode and the carbon rod were used as the reference and counter electrodes, respectively. The voltages on the disk electrode and ring electrode are open circuit voltage and 0.9 V vs. SCE. The scan rate of 10 mV·s$^{-1}$.

**S9. The calculation of HOMO and LUMO levels.**

The measurement of CV curve was carried out in acetonitrile solution containing tetrabutylamine hexafluorophosphate (TBAP) saturated with nitrogen, ferrocene as the standard, glassy carbon electrode, $Ag/Ag^{+}$ electrode and carbon rod as the working electrode, reference electrode and counter electrode, respectively. The calculation formula is as follows:

$$E_{HUMO} = -(E_{onset}^{ox} - E_{ferrocene} + 4.8) \quad (5)$$

$$E_{LUMO} = -(E_{onset}^{red} - E_{ferrocene} + 4.8) \quad (6)$$

**Supplementary Figures**

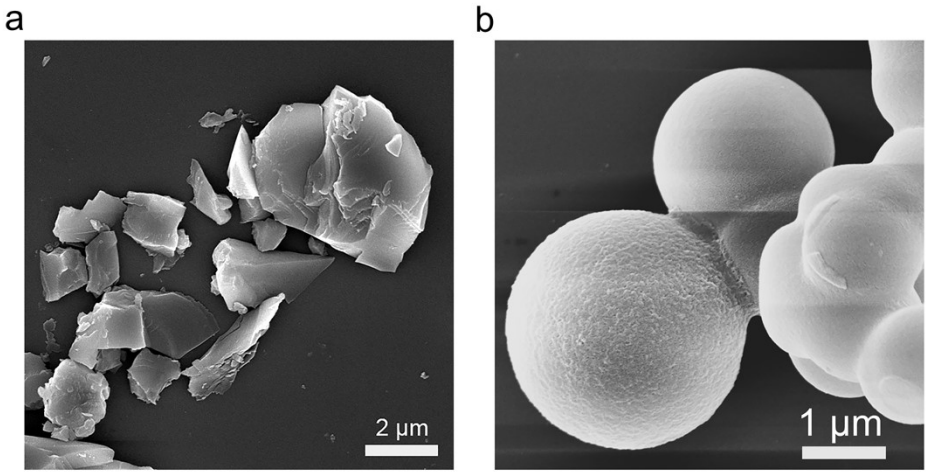


**Figure S1.** SEM images of (a) DEX-0 and (b) DEX-160.

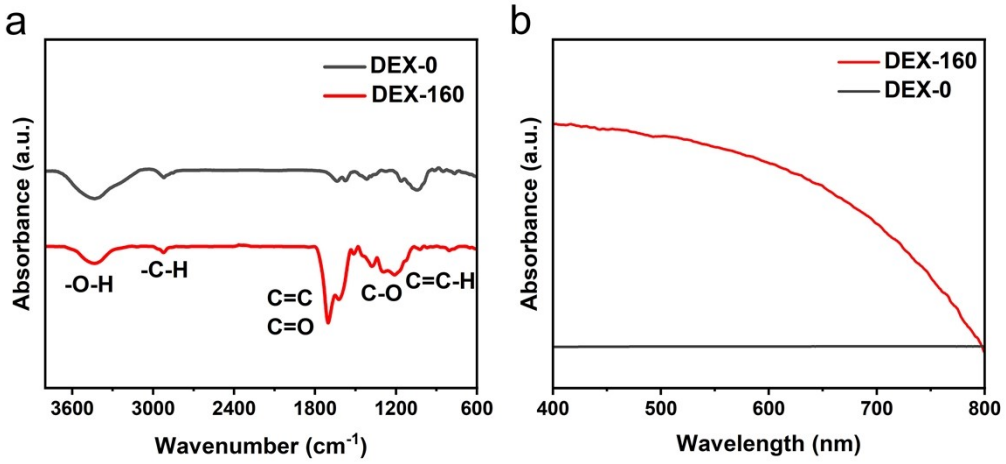


**Figure S2.** (a) FT-IR spectra of DEX-160 and DEX-0. (b) The UV-Vis absorption spectra of DEX-160 and DEX-0.

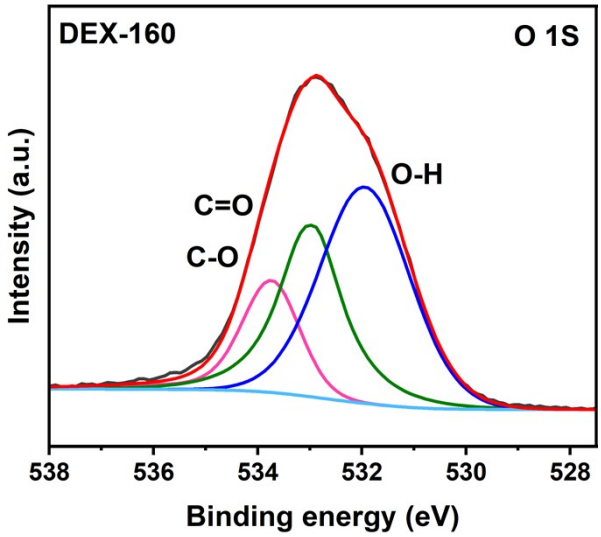


**Figure S3.** XPS spectra of DEX-160 for O 1s

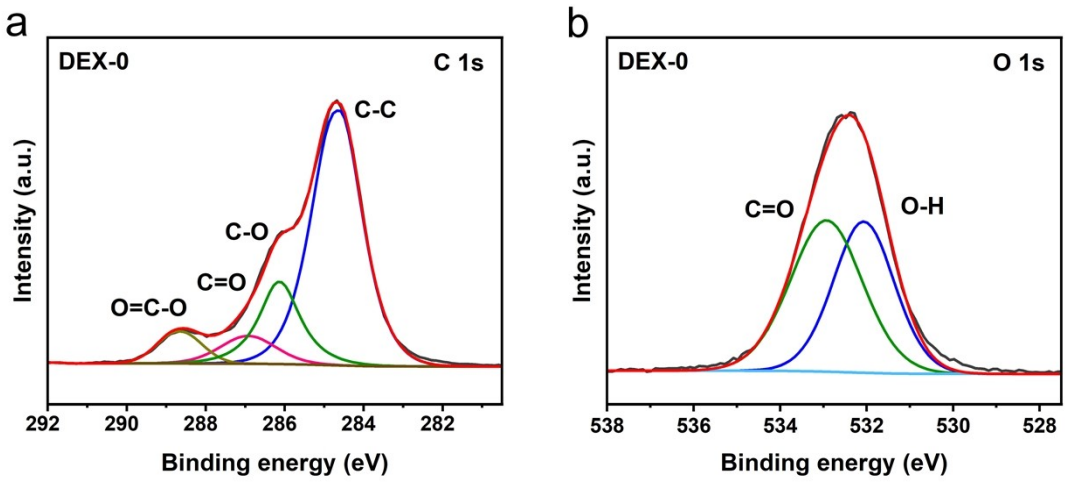


**Figure S4.** XPS spectra of DEX-0 for (a) C 1s and (b) O 1s

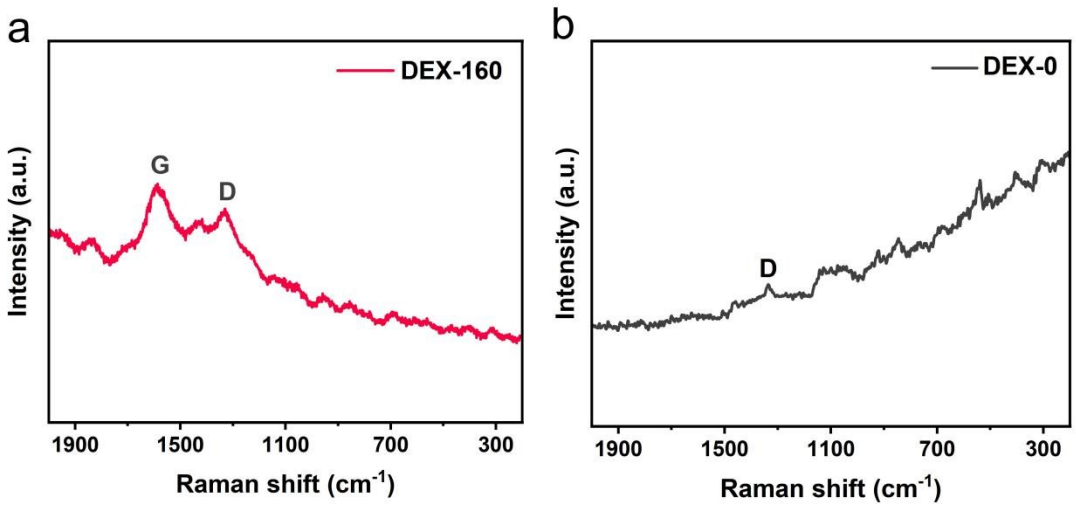


**Figure S5.** Raman spectra of (a) DEX-160 and (b) DEX-0.

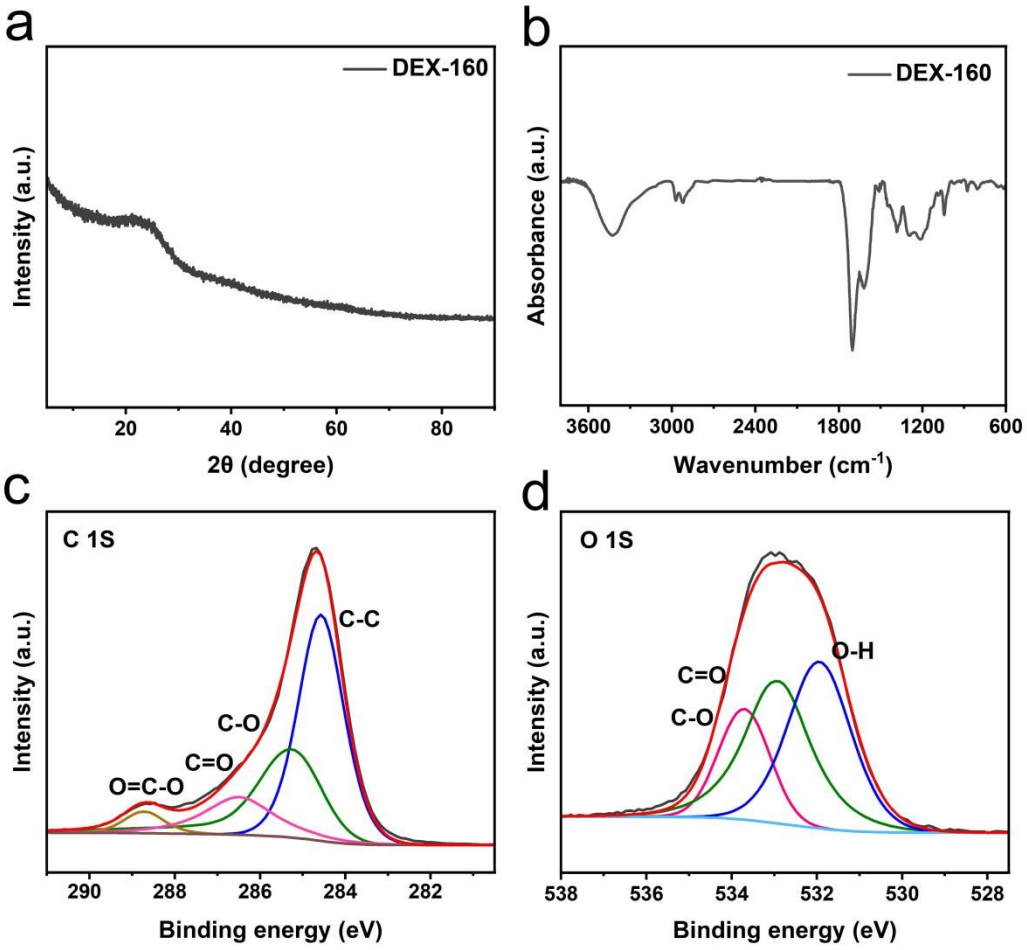


**Figure S6.** (a) XRD pattern, (b) The FT-IR spectrum, (c) C 1s and (d) O 1s XPS spectra of DEX-160 after irradiation for 5h.

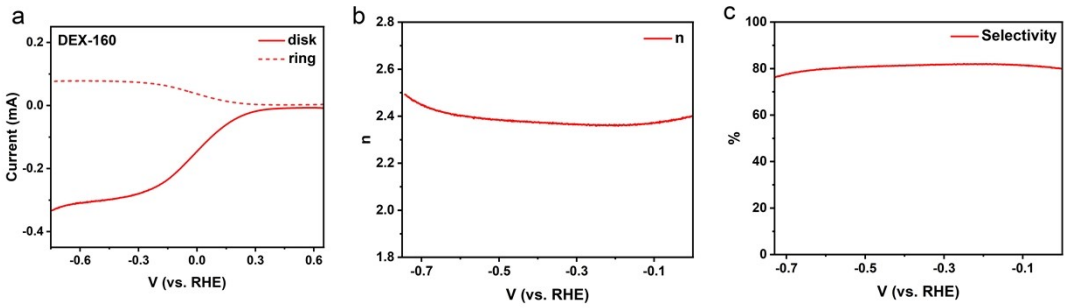


**Figure S7.** (a)The RRDE curves of DEX-160 tested in 0.1 M $Na_2SO_4$. (b) Number of transferred electron and (c) selectivity of oxygen reduction reaction with DEX-160.

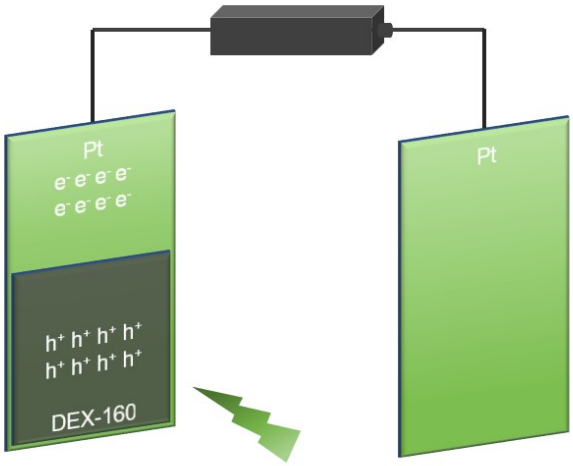


**Figure S8**. The schematic diagram of TPV test system.

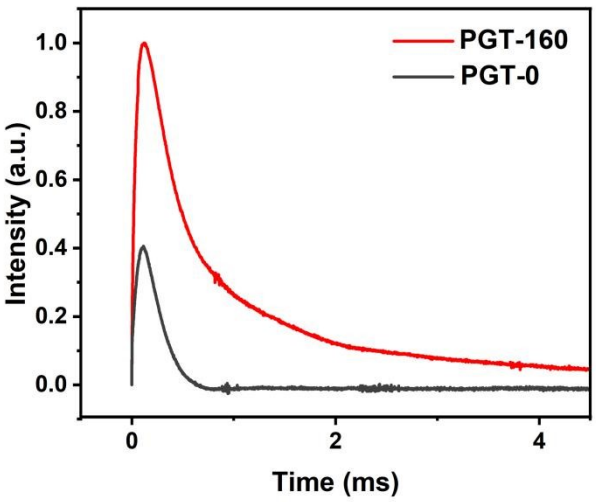


**Figure S9.** TPV curves used to conduct FFT and CWT.

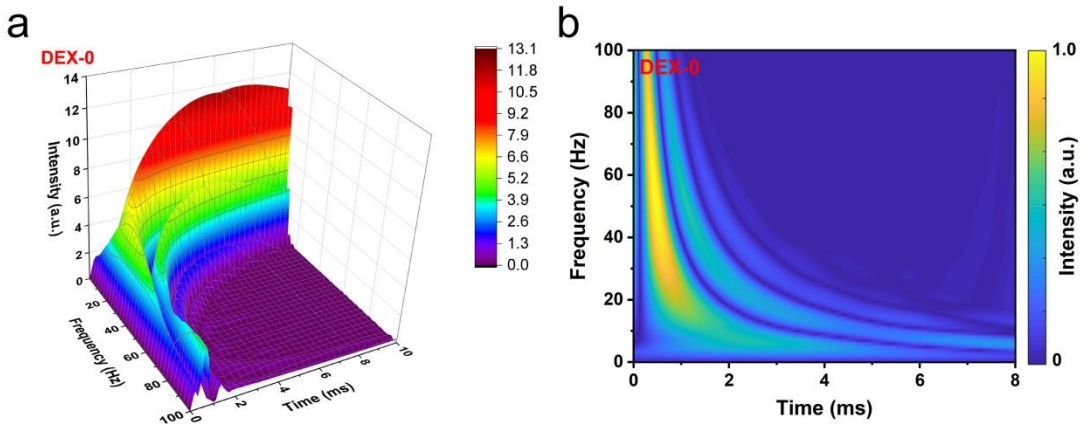


**Figure S10.** 3D and 2D CWT spectra of DEX-0.

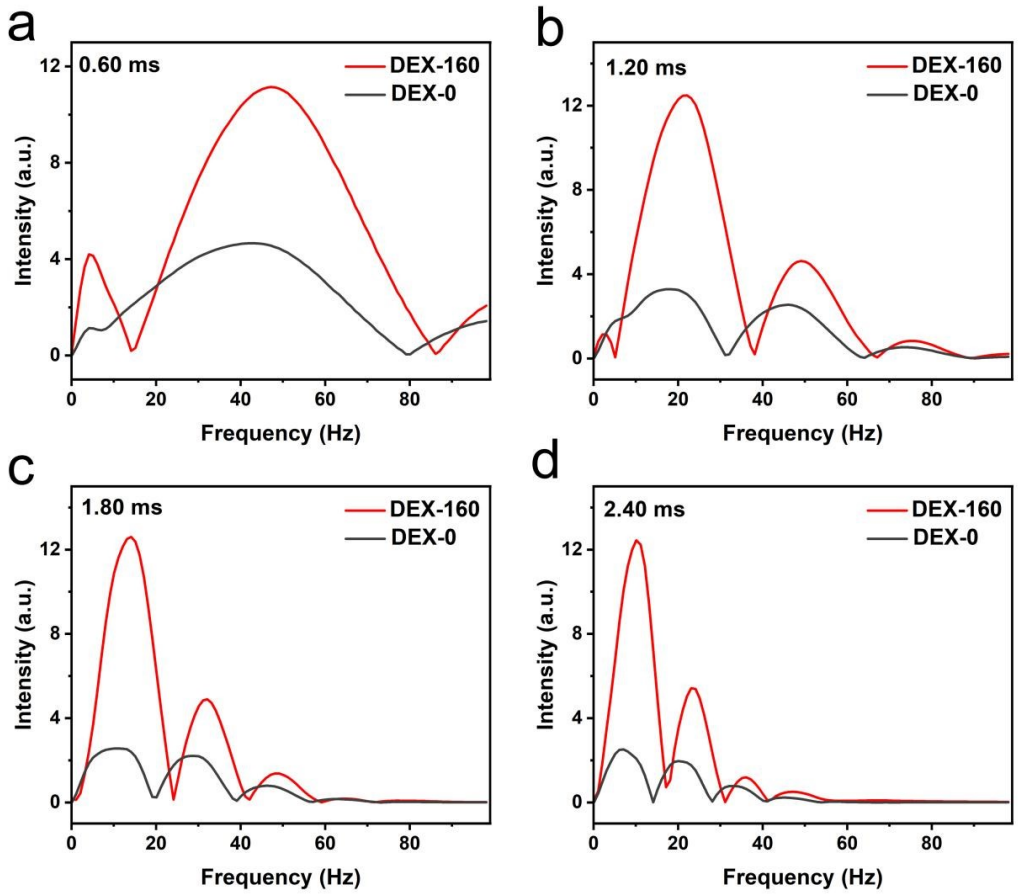


**Figure S11.** Frequency-Intensity curves (t = 0.06, 1.20, 1.80 and 2.40 ms) of DEX-0 and DEX-160.

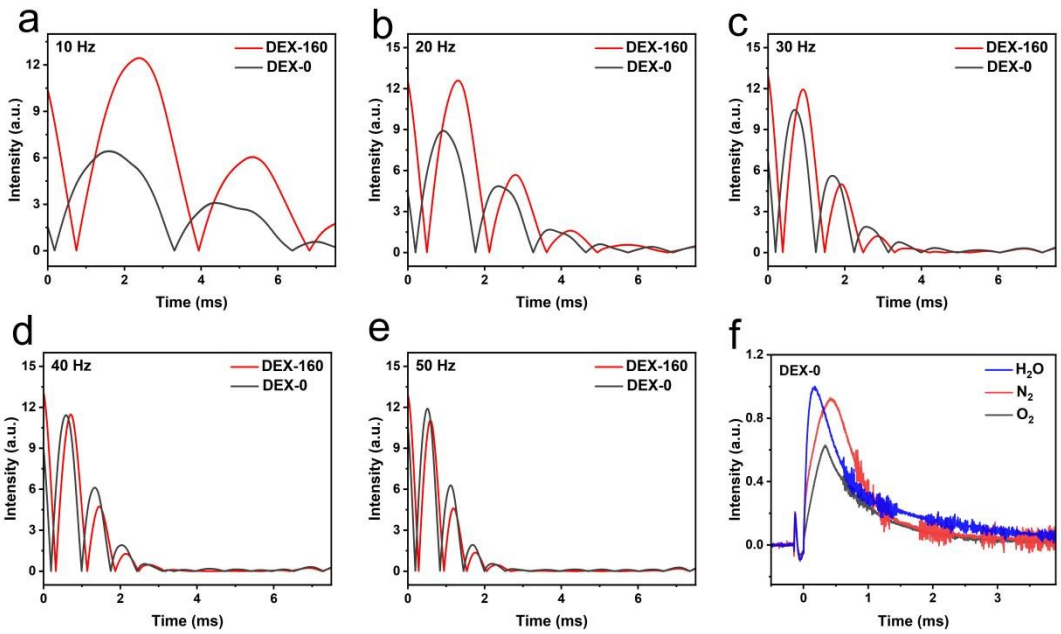


**Figure S12.** (a)-(e) Time-intensity curves (f = 5, 10, 15, 20, 25, 30, 35, 40, 45, 50 Hz) of DEX-0 and DEX-160. (f) TPV curves of DEX-0 in $H_2O$, saturated $N_2$ and $O_2$.

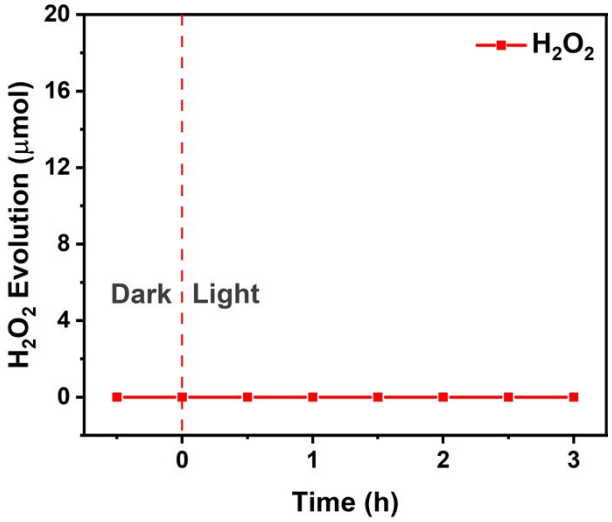


**Figure S13.** Detection of $H_2O_2$ production in different time when adding DEX-0.

## Supplementary Tables

**Table S1.** The comparison of $H_2O_2$ production with DEX-160 as photocatalyst and recently reported.

| Material | Sacrificial reagent | Irradiation conditions | $H_2O_2$ yield | Ref. |
|---|---|---|---|---|
| $TiO_2$ | 2-propanol | λ=365 nm | 86 μM $min^{-1}$ | S1 |
| Au/$TiO_2$ | ethonal | λ>300 nm | 17 mM (23 h) | S2 |
| N-doped $TiO_2$ | none | λ=422 nm | 5 nM $min^{-1}$ | S3 |
| Au-Ag/$TiO_2$ | ethonal | λ=280 nm | 3.7 mM (24 h) | S4 |
| g-$C_3N_4$/$TiO_2$ | phenol | visible | 110 μmol (2 h) | S5 |
| ZnO | estrone | λ=365 nm | 1.58 μM (6 h) | S6 |
| g-$C_3N_4$/CuO | none | 400-800 nm | 6.9 μM (6 h) | S7 |
| g-$C_3N_4$/BDI | $H_2O$ | λ> 420 nm | 41 μmol (48 h) | S8 |
| g-$C_3N_4$/AQ | 2-propanol | Simulated solar | 361 μmol $g^{-1}$ $h^{-1}$ | S9 |
| Au/$BiVO_4$ | $H_2O$ | λ> 420 nm | 40.2 μmol (10 h) | S10 |
| Au/ZnO | ethanol | UV | 1.5 mmol $L^{-1}$ $h^{-1}$ | S11 |
| **DEX-160** | **$H_2O$** | **λ> 420 nm** | **2667 μmol $g^{-1}$ $h^{-1}$** | **This work** |

## References


S1 B. O. Burek, D. W. Bahnemann and J. Z. Bloh, *ACS Catal.*, 2018, **9**, 25-37.

S2 M. Teranishi, S.-i. Naya and H. Tada, *J. Phys. Chem. C*, 2016, **120**, 1083-1088.

S3 T. Hirakawa and Y. Nosaka, *J. Phys. Chem. C*, 2008, **112**, 15818-15823.

S4 D. Tsukamoto, A. Shiro, Y. Shiraishi, Y. Sugano, S. Ichikawa, S. Tanaka and T. Hirai, *ACS Catal.*, 2012, **2**, 599-603.

S5 A. Behera, P. Babu and K. Parida, *Inorg. Chem. Front.*, 2021, **8**, 1489-1499.

S6 Y. Liu, J. Han, W. Qiu and W. Gao, *Appl. Surf. Sci.*, 2012, **263**, 389-396.

S7 J. Bai, Y. Sun, M. Li, L. Yang, J. Li and S. Hu, *New J. Chem.*, 2018, **42**, 13529-13535.

S8 Y. Kofuji, S. Ohkita, Y. Shiraishi, H. Sakamoto, S. Tanaka, S. Ichikawa and T. Hirai, *ACS Catal.*, 2016, **6**, 7021-7029.

S9 H.-i. Kim, Y. Choi, S. Hu, W. Choi and J.-H. Kim, *Appl. Catal., B*, 2018, **229**, 121-129.

S10 H. Hirakawa, S. Shiota, Y. Shiraishi, H. Sakamoto, S. Ichikawa and T. Hirai, *ACS Catal.*, 2016, **6**, 4976-4982.

S11 X. Meng, P. Zong, L. Wang, F. Yang, W. Hou, S. Zhang, B. Li, Z. Guo, S. Liu, G. Zuo, Y. Du, T. Wang and V. A. L. Roy, *Catal. Commun.*, 2020, **134**, 105860.